FULL PAPER

Nanoshuttered OLEDs: Unveiled Invisible Auxiliary Electrode

Yong Sub Shim, Ju Hyun Hwang, Hyun Jun Lee, Kyung Bok Choi, Kyu Nyun Kim, Cheol Hwee Park, Sun-Gyu Jung, Young Wook Park, and Byeong-Kwon Ju**

In this study, organic light-emitting diodes (OLEDs) with enhanced optical properties are fabricated by inserting a nanosized stripe auxiliary electrode layer (nSAEL) between the substrate and an indium tin oxide (ITO) layer. This design can avoid the shortcomings of conventional microsized layers while maintaining high optical uniformity due to the improved conductivity of the electrode. The primary advantage is that the nSAEL (submicrometer scale) is no longer visible to the naked eye. Moreover, the reflective shuttered (grating) structure of the nSAEL increases the forward-directed light by the microcavity (MC) effect and minimizes the loss of light by the extracting the surface plasmon polariton (SPP) mode. In this study, the degree of the MC and SPP can be controlled with the parameters of the nSAEL by simply conjugating the conditions of laser interference lithography (LIL). Therefore, the current and power efficiencies of the device with an nSAEL with optimized parameters are 1.17 and 1.23 times higher than the reference device at 1000 cd/m^2, respectively, and at these parameters, the overall sheet resistance is reduced to less than half (48%). All of the processes are verified by comparing the computational simulation results and the experimental results obtained with the actual fabricated device.

1. Introduction

Organic light-emitting diodes (OLEDs) are being increasingly used in mainstream display and lighting applications because of their high energy efficiency, broad color gamut, fast response time, and applicability for flexible displays.[1–3] Extensive studies have been conducted on their potential applications in industrial and academic fields; however, many technical issues still exist. Because there is always a trade-off between the transparency and the conductivity of an electrode, the limiting conductivity of a highly transparent electrode such as a conventional indium tin oxide (ITO) electrode results in nonuniform current injection in large-panel fabrication. Consequently, problems such as inhomogeneous light emission and increased heat generation at the edge lead to a reduction in the lifetime of the device.[4] On the other hand, using a thin metallic electrode with high conductivity does not yield satisfactory optical efficiency because of its very low transparency.[5]

To overcome these problems, a microsized auxiliary electrode was proposed to enhance the optical and thermal properties of OLED devices.[6] However, several problems still exist. Shadow-mask patterning is not acceptable for a large-area panel display, and an excessively large auxiliary electrode is clearly visible in low-luminance environments. Additionally, an additional insulating process that enlarges the nonemissive region is required to prevent current concentration around the auxiliary electrodes because of the wide spacing between the wiring.

Recently, researchers have patterned thin metallic electrodes such as periodic nanohole arrays to increase transparency while retaining good conductivity.[7] These electrodes also have great potential for use in flexible optoelectronic devices because of the use of thin metals with good ductility. On the other hand, a flawless layer of patterned electrodes cannot be easily fabricated in a nanoscale process; consequently, the risk of a disconnection problem always exists. The greatest disadvantage of a nanoscale periodic pattern is that it can introduce a prism-like photonic-crystal effect, which causes serious spectrum distortion. Technical limitations such as the complexity of the process and disadvantages including high haze still exist though spectrum distortions can be minimized by reducing the pitch below visible wavelengths and by using a diffuser (including a microlens array).[8] Moreover, this process is only applicable to highly transparent and expensive metals such as silver, which are unsuitable for industry.

In this study, we investigated a nanosized stripe auxiliary electrode layer (nSAEL) that is applicable to even impermeable and

Y. S. Shim, J. H. Hwang, H. J. Lee, K. B. Choi, K. N. Kim, C. H. Park, S.-G. Jung, Prof. B.-K. Ju
Display and Nanosystem Laboratory
College of Engineering
Korea University
Seoul 136–713, Republic of Korea
E-mail: bkju@korea.ac.kr
Prof. Y. W. Park
The institute of High Technology Materials and Devices
Korea University
Seoul 136–713, Republic of Korea
E-mail: zerook@korea.ac.kr

DOI: 10.1002/adfm.201401253

low-cost metals, specifically Al. The high conductivity of Al leads to a reduction in the overall sheet resistance, and a relatively high optical efficiency can be obtained from an OLED device with opaque auxiliary electrodes by increasing the forward-directed light using the MC effect[9] and by minimizing spectral variations via a finite-difference time-domain (FDTD) simulation and actual device fabrication. This type of nanopatterned electrode can also be used to fabricate OLEDs with a more corrugated structure and can enhance the optical properties in terms of the geometrical optics[10,11] and varying the SPP mode to an out-coupling mode resulting from the grating structure.[12,13] The risk of disconnection is sufficiently diminished because the nSAEL is merely an assistance layer for the ITO electrode. The wiring of the nSAEL is invisible; thus, it resembles a thin film, and this process is easy and suitable for large-area processing via a laser interference lithography (LIL) process.

2. Results and Discussion

2.1. Fabrication and Characterization of nSAEL

The entire fabrication process is shown in **Figure 1**. We fabricated an nSAEL on a glass substrate using an LIL process. First, negative photoresist (PR) was spin coated on a glass substrate and then exposed for fine patterning via a laser. Different shapes of the negative PR were patterned by regulating the conditions of the LIL process. A frequency-doubled Ar-ion laser with a wavelength of 257 nm was used, and the specific details are shown in **Figure 2**. While adjusting the laser exposure energy (25 mJ/cm^2) and the angle of the Lloyd's interference mirror (15°), the period of the pattern (referred to as the pitch) was maintained at a constant value for all experimental devices. Only the develop time (80–200 s) of the negative PR determines the ratio of the remaining area. The shape of the PR changes from a rectangle to a trapezoid (undercut edge profile), which has a sharp taper angle, as the develop time increases, as shown in the inset of **Figure 3**.

After the PR was formed, the Al for the nSAEL was deposited using the vacuum thermal evaporation method. Because Al strongly adheres to glass, only the portion deposited on the PR can be removed in an ultrasonic bath of acetone. After this lift-off process was completed, Al partially remained on the substrate as intended and formed the nSAEL.

Figure 3a–d show that the fine pattern of the auxiliary electrode was successfully fabricated. The width of the nSAEL was adjusted by controlling the bottom side length of the PR. The pitch and fill factor (FF) can be given as follows:[14]

$$\text{pitch} = \frac{\lambda_{\text{Ar}}}{2\sin\theta} \tag{1}$$

$$\text{fill factor} = \frac{\text{width of auxiliary electrode}}{\text{pitch}} \tag{2}$$

where θ is the incident angle for the Lloyd's interference mirror, and λ_{Ar} is the wavelength of the Ar-ion laser. In this work, the pitch of the auxiliary electrode was fixed (approximately 500 nm), and devices with different FFs (depending on the width of the auxiliary electrode) were fabricated. The FF can be varied from 0.30 to 0.80 depending on the develop time.

Figure 4a,b show the variation in the optical transmittance of the anodes of OLEDs with an nSAEL with an Al thickness in the visible-light region. Aluminum was evaporated to two thicknesses (15 nm and 30 nm) to investigate the correlation between the thickness and the degree of multipeaked spectral distortion. As the FF value increases, the optical transmittance decreases gradually at regular intervals. Although the thickness of the nSAEL does not significantly affect the average transmission of visible light, a prominent multipeak phenomenon can be seen at the wavelength that satisfies Bragg's diffraction law for the anode with a 30-nm-thick nSAEL when compared with an nSAEL that is less than 15-nm thick. The peak wavelength depends on the relationship between the guiding wavelength of the waveguide modes and Bragg's diffraction condition in a periodic structure.[15,16] To minimize this unintended effect caused by the photonic crystal structure, we employed a 15-nm-thick Al layer for the auxiliary electrodes of the fabricated OLEDs to ensure uniform permeability at visible wavelengths.

As shown in **Figure 5**, the nSAEL resembles a thin film. This structure can reduce the disadvantages of the clearly visible wiring in conventional microsized auxiliary electrodes.

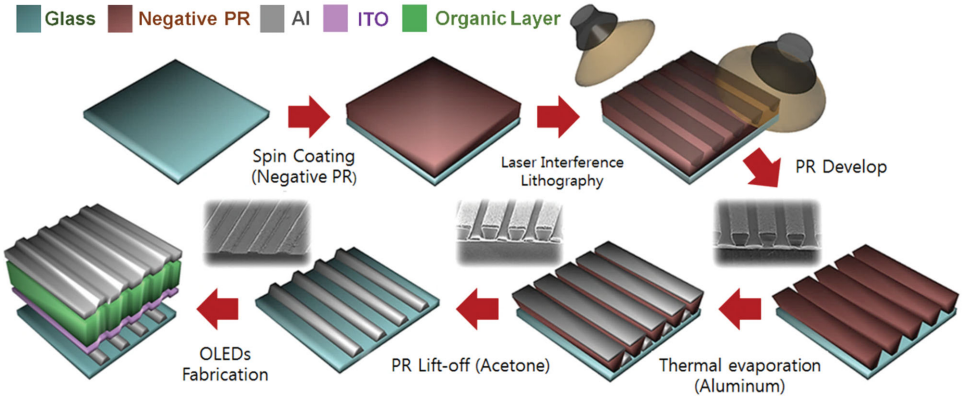

Figure 1. Schematic diagrams and SEM images (inset) of the fabrication process of OLEDs with an nSAEL.

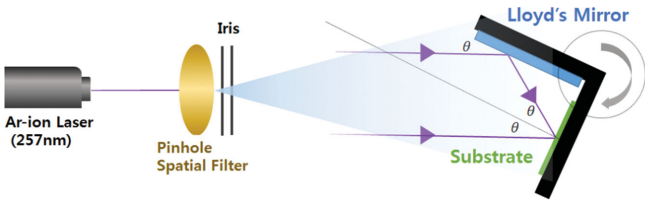

Figure 2. Illustration of the LIL system with a Lloyd's mirror interferometer.

Because the wiring of a nanosized auxiliary electrode is more evenly spread than that of a microsized electrode, the nSAEL has a low uniform distribution of sheet resistance, and the current density is not highly concentrated only around the auxiliary electrode without an additional insulating layer,[6,17] thus indicating that the non-emitting area caused by the insulating region is positively reduced. The measured sheet resistance is inversely proportional to the FF between 50 Ω/square with only the ITO layer (FF = 0) and 7 Ω/square with the ITO layer with 15-nm-thick fully packed Al (FF = 1.00), as shown in the inset of Figure 4. In other words, the overall sheet resistance is reduced rapidly by half at low FFs (0–0.3). Thereafter, for FF = 0.3–1, the curve decreases linearly with a small slope.

2.2. Simplified Patterned Microcavity Design for OLED

For electro-optical analysis, we fabricated OLEDs with different FFs. For OLEDs with nSAELs having different FFs, the MC effect is an important factor because the metallic area coverage ratio impacts the phase change at the cavity surface. Because the resonant wavelength of an MC OLED is determined by its vertical cavity length, the following simplified resonance equation can be used to fabricate an optimized MC device:[18–20]

$$\frac{2\pi}{\lambda}(2nd) - \varphi_1 - \varphi_2 = 2\pi m \tag{3}$$

where λ is the wavelength of the emitted light, and n is the average refractive index of the materials inside the cavity range. Further, φ is the phase change at cavity surface, and d is the vertical cavity length [in our devices, d = Thickness $_{(ITO)}$ + Thickness $_{(organic\ layers)}$]. The ITO layer thickness is included in the vertical cavity length because it is evaporated over the nSAEL as opposed to a conventional auxiliary electrode.[6,9] This structure has two major advantages. The ineffective carrier injection from Al to *N,N′*-bis(naphthalen-1-yl)-*N,N′*-bis(phenyl)-benzidine (NPB) is prevented by changing the interface from ITO to NPB, and the ITO layer thickness that affects the vertical cavity length has lesser impact on the carrier balance in OLEDs than the thicknesses of other organic layers. Therefore, to take advantage of the most significant effects of the MC for green emissions without any variations in carrier injection, the vertical cavity length was adjusted by varying ITO thickness. In Equation 3, the value of φ_2 can be assumed to be zero for low-FF devices whose cavity surfaces are primarily ITO or glass components, whereas for high-FF devices whose cavity surfaces are mainly metallic components, it can be assumed to be π. In the former case, when λ = 550 nm, n = 1.7, $\varphi_1 = \pi$, and φ_2 = 0, we obtain d = 240 nm (m = 1, referred to as $3\lambda/4n$ design), and in the latter case, for $\varphi_2 = \pi$ with the other values being constant, we obtain d = 160 nm (m = 0, referred to as $\lambda/2n$ design). In the latter case, a 160-nm-thick vertical cavity length is too small to

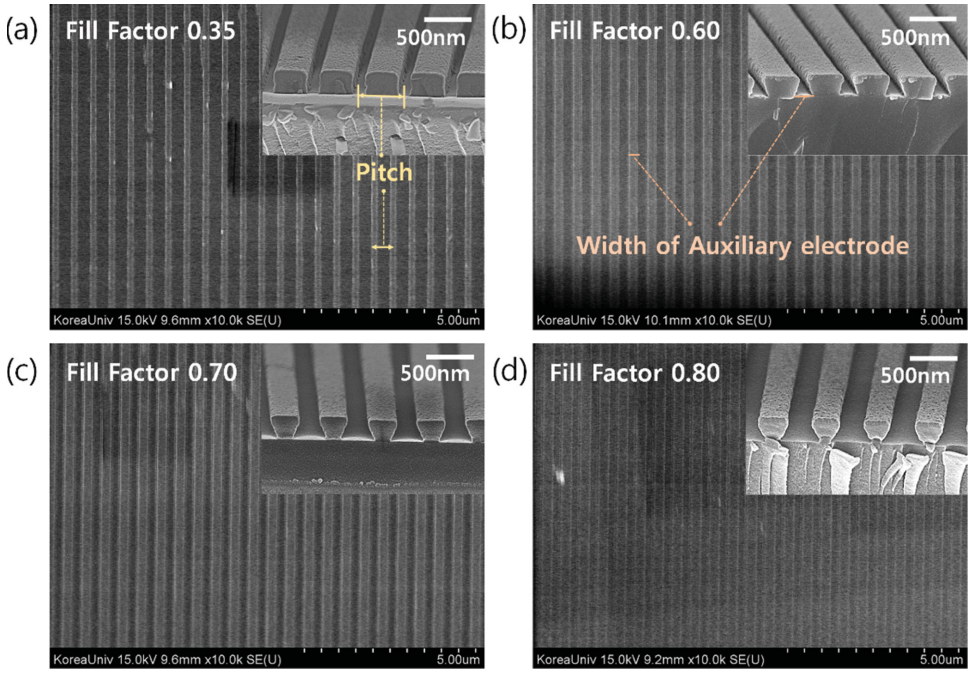

Figure 3. SEM images of the nSAEL. After the PR lift-off process, only the stripe-patterned Al auxiliary electrodes with different FFs remain. nSAELs with different PR shapes (inset) with develop times of a) 80 s (FF = 0.35), b) 120 s (FF = 0.60), c) 160 s (FF = 0.70), and d) 200 s (FF = 0.80).

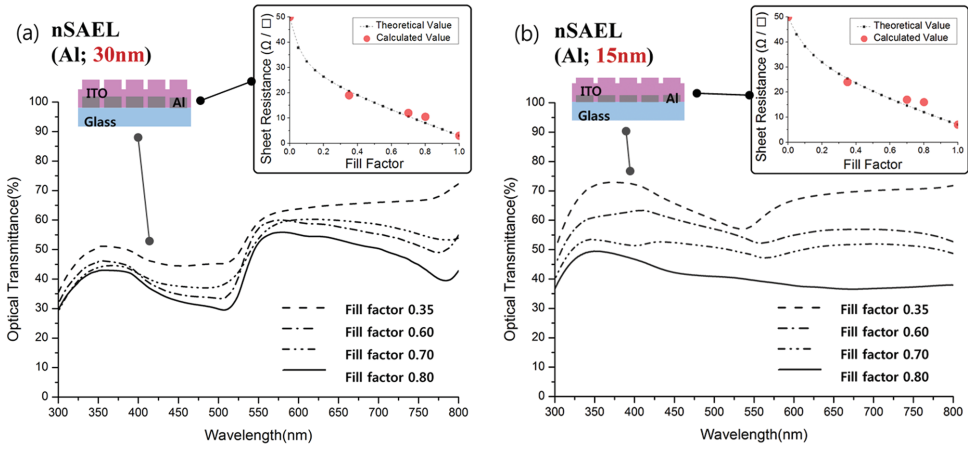

Figure 4. Plots of the optical transmittance versus wavelength and the sheet resistance versus FF (inset) for electrodes (anodes) of OLEDs with a) 30-nm-thick and b) 15-nm-thick nSAELs.

include both organic and ITO layers. Moreover, because we use opaque materials (Al), which have high absorption ratio, as nSAELs, the optimal point at an extremely high FF cannot be determined because of the destruction of photons inside the OLEDs. Of course, adjusting the vertical cavity length to obtain a high-FF design can lead to a stronger cavity effect owing to the high reflectivity of Al. However, the focus of this study is to design an invisible auxiliary electrode despite using relatively the weak cavity surface of devices with low FF. Therefore, the d = 240 nm case was chosen for MC design.

2.3. Optical OLED Simulations

The MC and extracted SPP mode effects are known to coexist significantly in the range of visible wavelengths in patterned metallic structures such as nSAELs.[19] In this study, a computational simulation was used to compare the theoretical and actual performance of the fabricated device. The thickness of the ITO layer and the FF affecting the degree of MC and SPP were optimized using an FDTD tool that is suitable for measuring the optical characteristics of OLEDs with nanoscale periodic structures.[21] The simulation was performed by varying the ITO thickness from 40 nm to 160 nm (the thickness of the organic layers was fixed at 140 nm) and the FFs from 0 to 1. **Figures 6**a,c show the variation of relative enhancement ratio with an ITO thickness and FF at a green emission wavelength of 550 nm. Because only the optical properties were considered without considering the amount of current injected, the simulated results may differ slightly from the actual ratio. The simulation data were then used to analyze the relative trends of each nSAEL device. Despite a slight overestimation, a 100–120-nm-thick ITO layer (d = 240–260 nm) has the best relative enhancement ratio corresponding to the theoretical vertical cavity length expressed in Equation 3, and the metal coverage ratio affecting both the degree of MC and SPP was optimized at FF values of 0.3–0.4. More photons escaped directly owing to the MC effect, and at a specific wavelength and angle, increased light extraction was observed owing to the outcoupled SPP mode,[12,13] as can be clearly seen in Figure 6b.

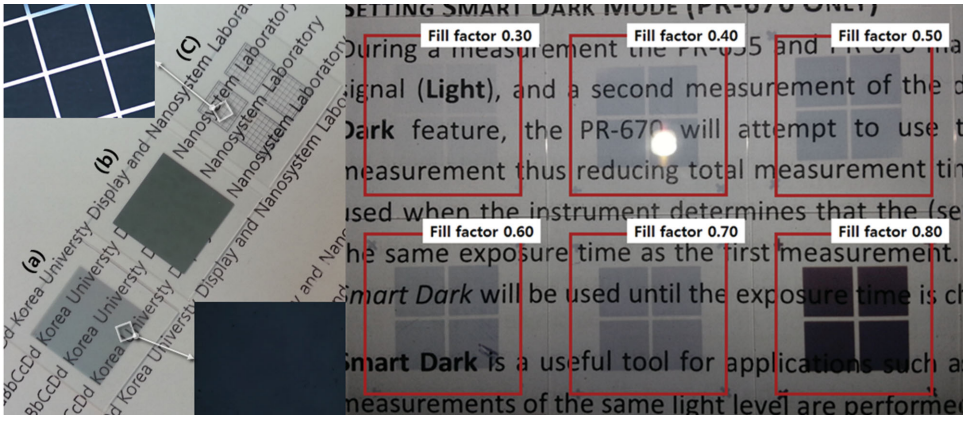

Figure 5. Left: Comparative photographs of the a) 15-nm-thick nSAEL, b) fully packed Al, and c) 15-nm-thick microsized auxiliary electrode. The inset shows the optical microscope images of each electrode observed at the same magnification. The wiring of the microsized auxiliary electrode is clearly visible, whereas that of the nanosized auxiliary electrode cannot be observed, even at the magnification of the optical microscope. Right: Photographs of nSAELs with FFs ranging from 0.30 to 0.80.

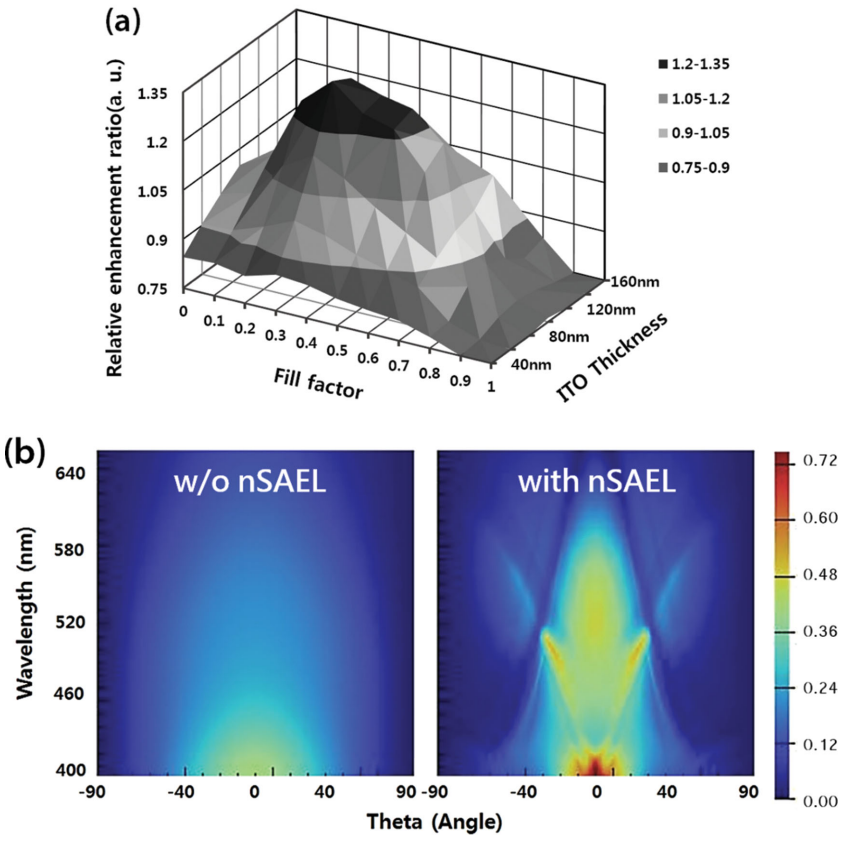

(c)

ITO Thickness (nm)

Fill factor	40nm	60nm	80nm	100nm	120nm	140nm	160nm
0	0.84	0.9	0.95	1.00	0.98	0.92	0.85
0.1	0.85	0.91	0.98	1.05	1.05	0.96	0.86
0.2	0.83	0.94	1.09	1.24	1.21	1.04	0.88
0.3	0.86	0.98	1.14	1.33	1.29	1.09	0.9
0.4	0.85	0.96	1.09	1.25	1.26	1.09	0.89
0.5	0.83	0.93	1.03	1.22	1.25	1.09	0.89
0.6	0.82	0.9	0.97	1.12	1.16	1.08	0.89
0.7	0.81	0.87	0.92	0.96	0.98	1.04	0.87
0.8	0.78	0.79	0.85	0.88	0.85	0.81	0.83
0.9	0.74	0.76	0.78	0.79	0.78	0.76	0.75
1	0.72	0.74	0.75	0.76	0.75	0.74	0.73

Figure 6. FDTD simulation results. a,c) The relative enhancement ratio as a function of ITO thickness and FF at 550 nm (range of viewing angle: inside a 30° cone). b) Verification of the increased directly escaped photons and extracted SPP mode for 100-nm-thick ITO with an FF of 0.3.

It should be noted that when FF is greater than 0.7–0.8, the efficiency is abruptly reduced, thus indicating that a critical point exists in this range. Because of the high absorption ratio of the opaque electrode (nSAEL created with Al) and a high degree of confined SPP mode due to the relatively flat Al surface, the photons are almost trapped inside the OLEDs beyond this critical point. A 240-nm-thick vertical cavity length is the condition at which constructive interference occurs in low-FF devices. In contrast, destructive interference occurs in high-FF devices. Therefore, the OLED model near this point is no more effective than an Al free (FF = 0) device.

In our study, the simulation design focused on low-FF devices to achieve sufficient transparency of the invisible auxiliary electrode. However, if the vertical cavity length is assumed to be exactly matched (160-nm thick) for high-FF devices, completely different results can be expected. The specific details of the simulation of the strong cavity design for high-FF devices are provided in the Supporting Information.

2.4. Electroluminescence Characteristics

Organic light-emitting diodes with FF values of 0, (used as a reference device) 0.3–0.4, (at which the maximum efficiency is achieved with the appropriate degree of MC and extracted SPP mode by grating), and 0.8 or higher, (the critical point at which efficiency is sharply reduced) were fabricated on the basis of the simulation results (**Figure 7**).

The electroluminescence (EL) characteristics of the OLED devices are shown in **Figure 8**. Figure 8a shows the variation of the current density with voltage. The current density of the devices having an nSAEL increased with higher FF values at the same bias voltage when compared with those without an nSAEL because of the influence of Al conductivity and an increase in the surface area of the electrode due to the nanosized stripe pattern.[10,22] The luminance versus voltage plot shows significant differences depending on the presence of the nSAEL. Therefore, the luminance is highest for a device with FF = 0.35 and lowest for a device with FF = 1.00 (fully packed Al) at the same current density. The increase in luminance in the devices with FF = 0.35 can be attributed to the fitted weak cavity resonant condition and the extracted SPP mode, which increases the number of extracted photons. Furthermore, the corrugated pattern of the organic layers created with the nSAEL was predicted to have a positive role in increasing the internal light extraction.[10,11]

As a result, we obtained four devices with different optical efficiencies due to their electrical characteristics. A summary of the current and power efficiency characteristics of the fabricated OLEDs is listed in **Table 1**. The current and power efficiencies of the FF = 0 (Al free), FF = 0.35, FF = 0.80, and FF = 1.00 (fully packed Al) devices were 3.79 cd/A (1.83 lm/W), 4.45 cd/A (2.25 lm/W), 3.59 cd/A (1.80 lm/W), and 3.13 cd/A (1.53 lm/W), respectively, at 1000 cd/m^2. The device with fully packed Al had the strongest reflective surface for the MC effect; however, a high current density, mismatched resonance condition, and the high absorption ratio of opaque Al resulted in the lowest efficiency, even when compared with the Al-free device. In accordance with the FDTD simulation results, the optimized FF was approximately 0.35 for the best performance. The efficiency improvement was

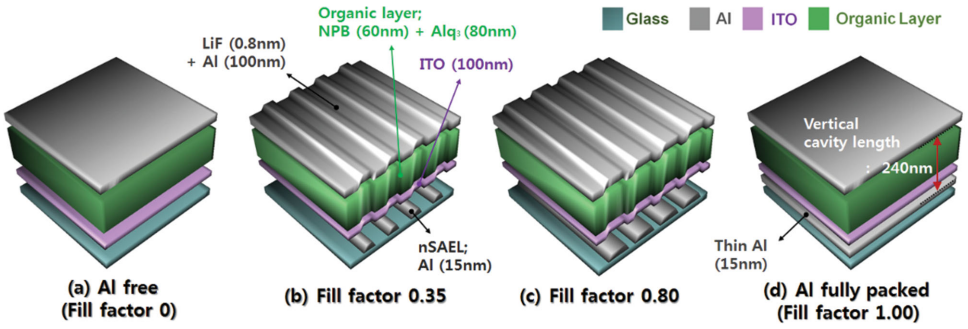

Figure 7. Schematic diagrams of the fabricated OLEDs: a) Al free (FF = 0), b) FF = 0.35, c) FF = 0.80, and d) fully packed Al (FF = 1.00).

not very high in the optimized device; however, these results are meaningful in aspect of obtaining a high-performance despite of utilizing the opaque auxiliary electrode for achieving uniform emissions and lifetimes of the devices.[6]

Figure 8c shows the normalized EL spectra of the four devices at a current density of 100 mA/cm^2. The reflective properties of the nSAEL reduced the width of the emission spectrum and caused slight variations in the spectral peak. These spectral variations are significant as FF increases, and the strongest variations occurred in the device with fully packed Al (FF = 1.00).[9] The variations show a gradual tendency from Al free (FF = 0.00) to fully packed Al (FF = 1.00) conditions, as shown in the figure. Consequently, only a few minor variations can be observed in the peak and width of the spectrum of the most optically efficient device, namely for FF = 0.35.

This indicates that the coverage (the ratio covered by nSAEL, which is related to both MC and extracted SPP mode effects) area was optimized, and more light was extracted from the trapped photons without significant variations in the spectrum of the device for an FF of 0.35. Further, the simulated and experimental values are almost similar with similar peak FF values and wavelengths, as shown in Figure 8d. Finally, we were able to obtain a high-performance nSAEL device using an appropriate degree of MC and SPP by geometrically adjusting the metal coverage area in the LIL process.

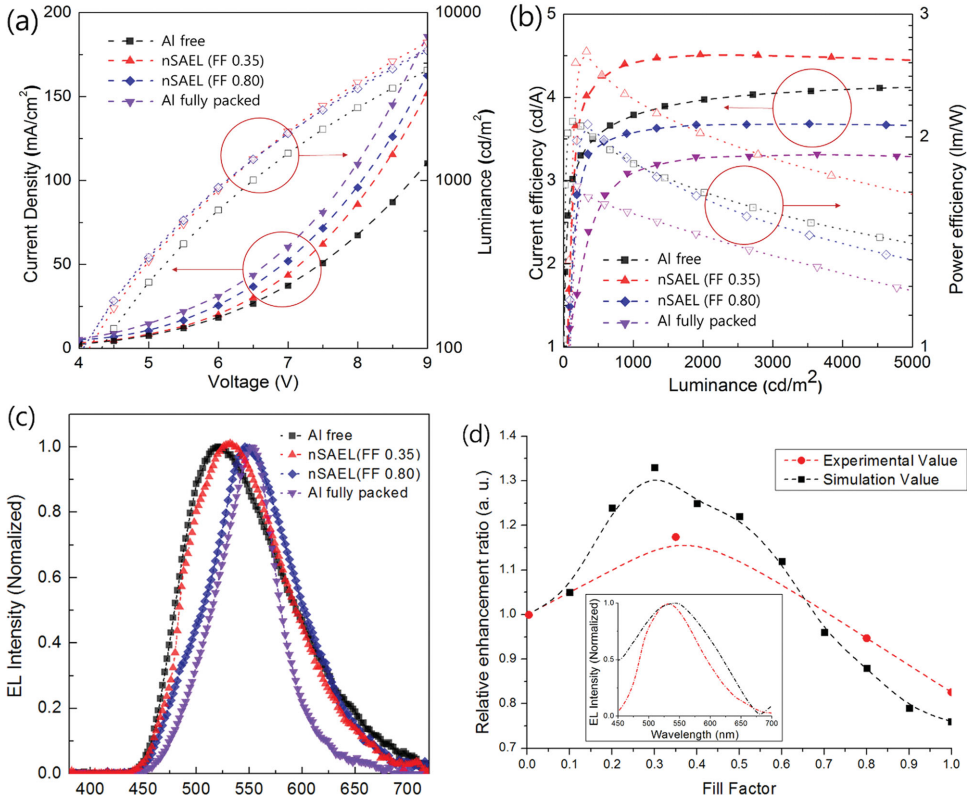

Figure 8. EL characteristics of the fabricated OLEDs. a) *I–V* and *V–L* characteristics of the devices. b) The current and power efficiency characteristics of the devices versus luminance. c) Normalized EL intensity of the devices. d) Comparison of the simulated and experimental enhancement ratios versus FF and (inset) comparison of the wavelength versus normalized EL intensity curves with FF = 0.35.

Table 1. Summary of the optical performance of fabricated OLEDs.

	Current efficiency [cd/A]		Power efficiency [lm/W]	
	at 1000 cd/m^2	at 3000 cd/m^2	at 1000 cd/m^2	at 3000 cd/m^2
Al free	3.79	4.05	1.83	1.54
nSAEL (FF 0.35)	4.45 (+17.4%)[a)]	4.50 (+11.1%)[a)]	2.25 (+23.0%)[a)]	1.88 (+22.1%)[a)]
nSAEL (FF 0.80)	3.59	3.67	1.80	1.48
Al fully packed	3.13	3.30	1.53	1.33

[a)]Enhancement ratios.

3. Conclusion

We fabricated a nanosized stripe auxiliary electrode that can be used for large-area OLEDs using the LIL method. We demonstrated improved optical efficiency despite adding an auxiliary electrode by optimizing the FF of the nSAEL (determining the degree of MC and SPP). All of the processes were verified by comparing the FDTD simulation results and the experimental results obtained with the actual fabricated device. The OLED device with a 100-nm-thick ITO layer with an nSAEL having an FF value of 0.35 exhibited the maximum optical efficiency with minimal spectrum variations. At this optimized point, the invisible property of the nSAEL was found to be fully satisfied. The greatest advantage of the nSAEL is that this process is widely applicable to even opaque metals such as Al and ensures a uniform current distribution for large-area OLEDs resulting from a reduced overall sheet resistance. Moreover, complex processes such as a thick insulator coating between an auxiliary electrode and an organic layer to prevent current concentration in conventional microsized devices, which result in non-emitting regions in devices, are no longer required. In summary, the simple, low-cost, large-area process involving an nSAEL has significant potential for mass-produced applications.

4. Experimental Section

Trapezoidal Profile (PR): Hexamethyldisilazane (HMDS) and a negative PR (AR-N 4240, Allresist Co., Ltd.) with a thinner (AR 300–12, Allresist Co., Ltd.) were spin coated for 40 s at 4000 rpm on an Eagle XG glass (Corning, Inc.) substrate and then annealed on a hot plate at 180° and 100°, respectively, for soft baking. The HMDS layer is a supplement for improved adhesion of the PR, and the thinner is mixed to create a thin PR (≈200 nm) for easy fine patterning. The PR was then exposed to a frequency-doubled Ar-ion laser (λ_{Ar} = 257nm, Power = 0.1 mW/cm^2) for 250 s and annealed on a hot plate at 90°. Different PR shapes (trapezoidal, undercut edge profile) were fabricated by varying the develop time (80–200 s).

OLED Fabrication: The anode (ITO) was deposited using radio-frequency sputtering, and the organic layers (small molecule) and cathode (Al) were evaporated using a thermal vacuum evaporator (10^{-6} Torr). The devices consist of a 15-nm-thick Al layer as an nSAEL, O_2-plasma-treated 100-nm-thick ITO layers as the main electrodes, a 60-nm-thick *N,N′*-Bis(naphthalen-1-yl)-*N,N′*-bis(phenyl)-benzidine (NPB) layer as a hole transport layer, a 80-nm-thick tris(8-hydroxyquinolinato) aluminum (Alq_3) layer as both an electron transport layer and an emissive layer, a 0.8-nm-thick lithium fluoride (LiF) layer as an electron injection layer, and a 100-nm-thick Al layer as a highly reflective cathode. The total resonant length from the ITO layer to the Alq_3 layer was 240 nm, which was consistent with the theoretical MC design.

Computational Simulation: Commercial FDTD software (Lumerical Solutions, Inc.) was used for simulation. Randomly distributed and oriented dipoles were estimated to apply the properties of the sheet light source of OLEDs. The relative enhancement ratio (light extraction) of each structure was calculated as the ratio of the optical power (from the Poynting vector) by a fixed far-field monitor. The specific details of the simulation are provided in the Supporting Information.

Spectral Measurement: The optical transmittances were measured with a Cary 5000 (Agilent Technologies Inc.) spectrophotometer, and the EL characteristics were measured using a PR-670 (SpectraScan, Photo Research, Inc.) spectroradiometer in a dark box (≈0.1 lx, at room temperature) with an adjustable voltage source (Model 237, Keithley Instruments, Inc.).

Supporting Information

Supporting Information is available from the Wiley Online Library or from the author.

Acknowledgements

This research was supported by the Basic Science Research Program through the National Research Foundation of Korea (NRF) funded by the Ministry of Education, Science and Technology (No. 2012R1A6A3A04039396), an NRF grant funded by the Korean government (MSIP) (CAFDC 4–2, NRF 2007–0056090), and the IT R&D program of the Development of Key Technology for Interactive Smart OLED Lighting, which is a part of the ETRI Internal Research Fund.

Received: April 18, 2014
Revised: June 27, 2014
Published online: August 21, 2014

[1] A. Sugimoto, H. Ochi, S. Fujimura, A. Yoshida, T. Miyadera, M. Tsuchida, *IEEE J. Sel. Top. Quantum Electron.* **2004**, *10*, 107–114.
[2] T. H. Kwon, Y. H. Oh, I. S. Shin, J. I. Hong, *Adv. Funct. Mater.* **2009**, *19*, 711–717.
[3] S. Reineke, F. Lindner, G. Schwartz, N. Seidler, K. Walzer, B. Lüssem, K. Leo, *Nature* **2009**, *459*, 234.
[4] H. Sasabe, J. Kido, *J. Mater. Chem.* **2013**, *C 1*, 1699.
[5] C. W. Chen, P. Y. Hsieh, H. H. Chiang, C. L. Lin, H. M. Wu, C. C. Wu, *Appl. Phys. Lett.* **2003**, *83*, 5127.
[6] J. Park, J. Lee, Y. Y. Noh, *Org. Electron.* **2012**, *13*, 184–194.
[7] Y. H. Ho, K. Y. Chen, K. Y. Peng, M. C. Tsai, W. C. Tian, P. K. Wei, *Opt. Express* **2013**, *21*, 8535–8543.

[8] K. B. Choi, S. J. Shin, T. H. Park, H. J. Lee, J. H. Hwang, J. H. Park, B. Y. Hwang, Y. W. Park, B. K. Ju, *Org. Electron.* **2014**, *15*, 111–117.
[9] J. Lee, H. Cho, T. W. Koh, S. Hofmann, Y. H. Kim, C. Yun, T. Schwab, S. Reineke, B. Lüssem, J. I. Lee, S. Yoo, K. Leo, M. C. Gather, *Org. Elect.* **2013**, *14*, 2444–2450.
[10] W. H. Koo, S. M. Jeong, F. Araoka, K. Ishikawa, S. Nishimura, T. Toyooka, H. Takezoe, *Nat. Lett.* **2010**, *4*, 222–226.
[11] Y. Sun, S. R. Forrest, *Nat. Photonics* **2008**, *2*, 483–487.
[12] P. A. Hobson, J. A. E. Wasey, I. Sage, W. L. Barnes, *IEEE J. Sel. Top. Quantum Electron.* **2002**, *8*, 378–385.
[13] S. Wedge, W. L. Barnes, *Opt. Express* **2004**, *12*, 3673–3685.
[14] M. Walsh, *On the Design of Lithographic Interferometers and Their Applications*, Ph.D. Thesis, MIT, September **2004**.
[15] K. Ishihara, M. Fujita, I. Matsubara, T. Asano, S. Noda, *Appl. Phys. Lett.* **2007**, *90*, 1111114.
[16] Y. C. Kim, Y. W. Song, Y. H. Lee, Y. R. Do, *J. Appl. Phys.* **2004**, *96*, 7629–7636.
[17] R. S. Cok, A. D. Arnold, D. Winters, OLED Display with Auxiliary Electrode, *US Patent 6,812,637 B2 2004*.
[18] M. S. Ünlü, *J. Appl. Phys.* **1995**, *78*, 607–639.
[19] R. Brückner, Zakhidov, A. R. Scholz, M. Sudzius, S. I. Hintschich, H. Fröb, V. G. Lyssenko, K. Leo, *Nat. Photonics* **2012**, *49*, 322–326.
[20] M. C. Gather, N. M. Kronenberg, K. Meerholz, *Adv. Mater.* **2010**, *22*, 4634–4638.
[21] A. Chutinan, K. Ishihara, T. Asano, M. Fujita, S. Noda, *Org. Electron.* **2005**, *6*, 3–9.
[22] M. Fujita, T. Ueno, K. Ishihara, T. Asano, S. Noda, *Appl. Phys. Lett.* **2004**, *85*, 5769–5771.